IET Radar, Sonar & Navigation

Special Issue Call for Papers

Be Seen. Be Cited.
Submit your work to a new IET special issue

Connect with researchers and experts in your field and share knowledge.

Be part of the latest research trends, faster.

Read more

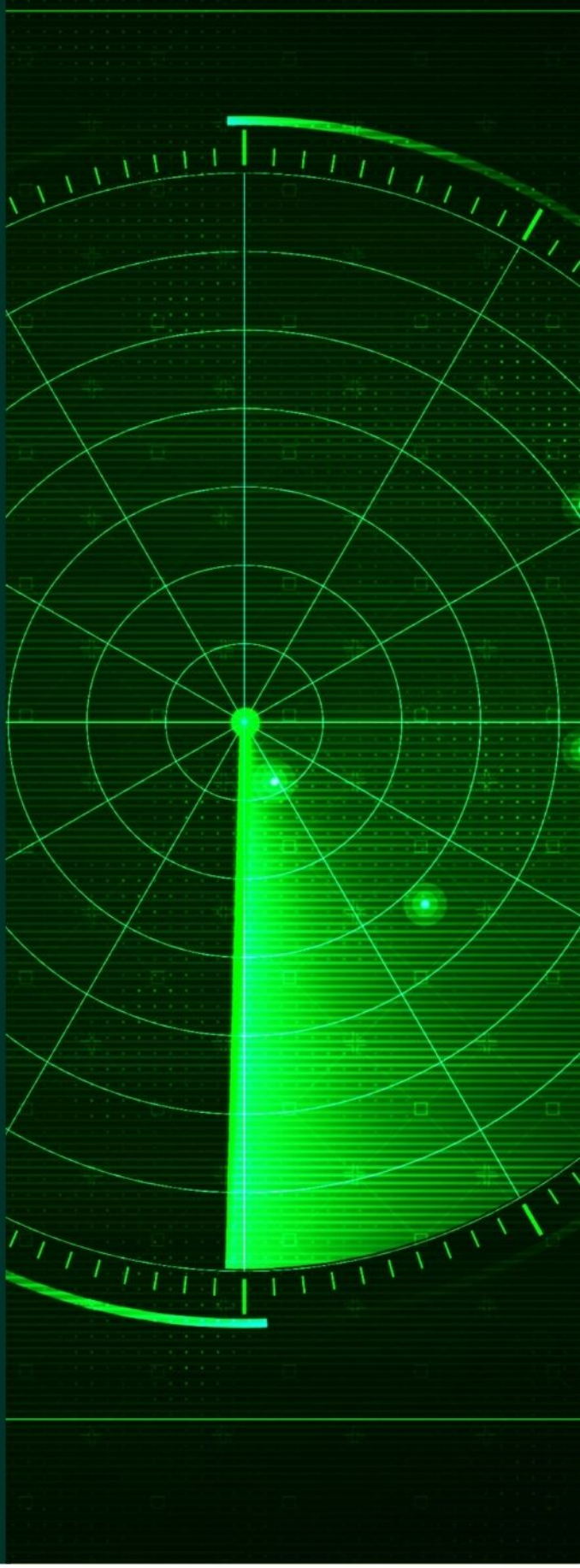

The Institution of Engineering and Technology

Received: 28 September 2022 | Revised: 19 May 2023 | Accepted: 7 July 2023

IET Radar, Sonar & Navigation

DOI: 10.1049/rsn2.12440

The Institution of Engineering and Technology WILEY

ORIGINAL RESEARCH

Choice and impact of frequency increment in direct digital synthesiser (DDS)-based linear FMCW radar

Paul Victor Brennan | **Lai Bun Lok**

Department of Electronic & Electrical Engineering, University College London, London, UK

Correspondence
Paul Victor Brennan.
Email: p.brennan@ucl.ac.uk

Abstract

FMCW radar is a popular technique for radar sensors. A Direct Digital Synthesiser (DDS) is commonly used to generate the required linear frequency sweep. DDS devices are widely-available and easy to configure in terms of the key radar parameters of sweep bandwidth and pulse duration. They generate a step-approximation to a linear frequency sweep for which the frequency increment parameter also needs to be defined. However, there is little information available in the literature to guide radar designers on the choice of this parameter. As a result, most designs are based on an empirical estimate of the DDS frequency increment. The aim is to provide an analytic basis and design rules for the choice of this parameter. Two principal types of FMCW radar (direct sampling and deramp) are studied to determine the effect on the range profile of the finite DDS frequency increment. It is shown that a set of spurs appears around each target response. Analytic expressions are derived to quantify the amplitude and distribution of these spurs from which simple design rules are presented to allow an informed choice of DDS frequency increment. These analytic results are convincingly validated using numerical simulations and experimental measurements.

KEYWORDS
FM radar, nonlinear systems, radar theory

1 | INTRODUCTION

Linear FMCW radar is a widely-used technique in radar sensors [1–3]. A Direct Digital Synthesiser (DDS) is almost invariably used to produce the frequency ramp, or chirp, for such a system [4–6], the DDS parameters being easy to configure in terms of the radar sweep bandwidth, B, and pulse duration, T, to satisfy the range/Doppler resolution and link budget requirements of a given FMCW radar system.

The DDS generates an approximation to a linear frequency ramp using discrete frequency steps or increments. The DDS frequency increment provides an independent and additional degree-of-freedom in the radar design, but unlike the standard radar parameters of bandwidth and pulse duration there is little or no clear guidance on the appropriate value that should be chosen for a given radar system and application. Porqueras et al. [7] applied the ambiguity function to suggest that a frequency increment less than $1/T$ can achieve similar detection performance to a theoretical linear chirp. Their approach, however, does not relate the choice of DDS frequency increment to the absolute level of degradation in detection performance and in most cases is a conservative estimate. Peek [8] considered the periodic digital phase errors of the step approximation to a linear chirp and suggests that the minimum possible DDS time increment is used as defined by the bit-resolution of the digital ramp rate register within the DDS and the system clock frequency [4–6], which is a very conservative approach constraining the choice of other DDS parameters in order to achieve the desired radar B and T values. As a result, DDS FMCW radar designers choose the DDS frequency increment value somewhat arbitrarily, generally making it smaller than necessary [8], thus causing unnecessary system constraints, or perhaps sometimes not small enough, resulting in avoidable performance degradation.

The purpose of this paper, therefore, is to address this area of DDS FMCW radar design by providing a simple and reliable set of analytic expressions, backed up by numerical simulation and measured results, to aid radar designers in determining an appropriate value of DDS frequency increment for a given application and performance requirement.

The paper considers the two principal architectures of FMCW radar: direct sampling, based typically on software-defined radio (SDR), Figure 1, and deramping, Figure 2. Performance analysis and design rules are presented for each architecture and are validated by numerical simulation and measurements. In particular, a very simple analytic expression is derived and validated for the required DDS frequency increment for acceptable performance.

The direct sampling FMCW radar architecture is illustrated in Figure 1. It comprises a DDS chirp generator that supplies the transmit linear frequency ramp (chirp) waveform along with a receive chain and ADC that directly samples the target responses at RF. DSP processing performs pulse compression and generates the range profile (target amplitude vs. distance). This is frequently implemented using an SDR [9].

The deramp FMCW radar architecture is illustrated in Figure 2. It comprises a DDS chirp generator that supplies both the transmit chirp waveform and a replica chirp, which is mixed with the target response in the receive path. The mixer output (the deramp signal) is sampled and FFT processing is applied to form the range profile. The direct sampling approach has the benefit of digital capture and processing of the signal at RF, providing flexibility and convenience, whereas the deramp approach involves a much lower sampling rate at the ADC leading to reduced power consumption and circuit complexity.

The pulse compression process in the direct sampling case is equivalent to multiplying the received target response by an ideal chirp of the same parameters as the transmit chirp, though this may instead be implemented by convolution in the frequency domain. The receive processing uses a perfect chirp waveform whilst the DDS provides a step-frequency approximation to a chirp, which is shown to lead to additional spurious components in the range profile.

The pulse compression process in the deramp case is effected by multiplying the transmit chirp with a set of delayed chirps from the various target responses. In this case, the step-frequency approximation to a chirp is involved in both the transmit and receive paths, which is shown to yield slightly different distribution of spurious components in the range profile.

The radar range resolution and deramp frequency for a target at range R are related to the radar sweep bandwidth, B, and pulse duration, T, by the well-known relations, which are given below [1]:

$$\text{Range resolution } \Delta R = \frac{c}{2B} \tag{1}$$

$$\text{Deramp frequency } f_d = \frac{2BR}{Tc} \tag{2}$$

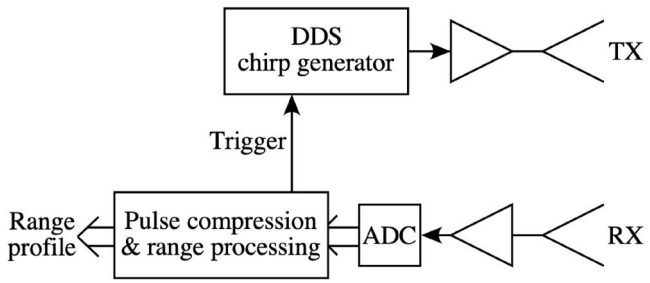

FIGURE 1 Simplified illustration of direct-sampling FMCW architecture.

2 | ANALYSIS OF THE IMPACT OF A FINITE DDS FREQUENCY INCREMENT AND DESIGN RULES

2.1 | Direct sampling linear FMCW radar

First considering the effect of the finite frequency increment, Δf (Hz), of duration ΔT (s) in a DDS chirp generator on the performance of a direct-sampling linear FMCW radar, typically based on an SDR platform.

Referring to Figure 3, the DDS step approximation to a continuous chirp results in a cyclic frequency error from the

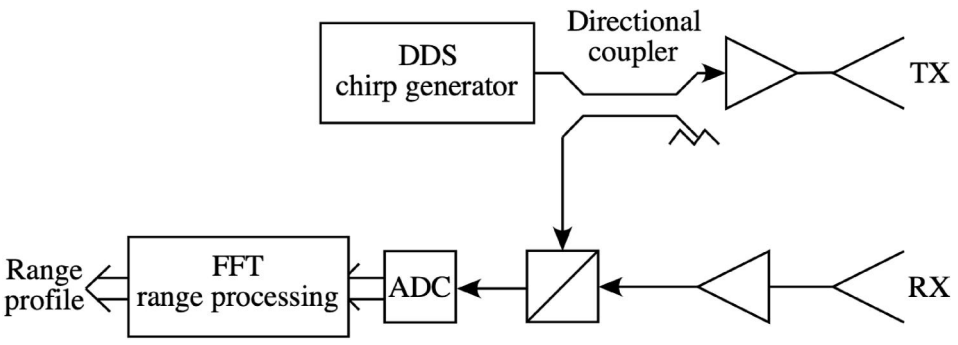

FIGURE 2 Simplified illustration of deramp FMCW architecture.

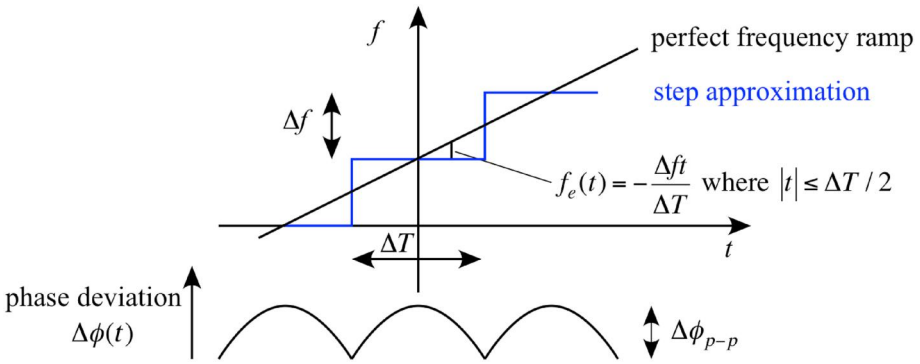

FIGURE 3 Direct Digital Synthesiser step-approximation to a continuous chirp.

ideal chirp with a triangular characteristic and a corresponding cyclic phase error with a parabolic characteristic. This introduces phase modulation on the transmitted chirp, which is effectively mixed with a perfect continuous chirp in the SDR receive processing, thus directly translating this phase modulation to the radar range return profile. The result is a set of characteristic spurious sidebands around each target response, of period ΔT and of frequency separation:

$$\Delta f_{\text{sideband}} = \frac{1}{\Delta T} \tag{3}$$

Since the DDS frequency increment, Δf, and time increment, ΔT, are related to the FMCW radar sweep bandwidth, B, and pulse duration, T, by the following:

$$\frac{\Delta f}{\Delta T} = \frac{B}{T} \tag{4}$$

then the frequency separation of these sidebands may also be written as follows:

$$\Delta f_{\text{sideband}} = \frac{B}{T\Delta f} \tag{5}$$

whilst the corresponding range sideband separation, using Equation (2), is given by the following:

$$\Delta R_{\text{sideband}} = \frac{cT}{2B}\frac{B}{T\Delta f} = \frac{c}{2\Delta f} \tag{6}$$

In terms of the magnitude of these spurious components, the frequency deviation between the step approximation to a frequency ramp and a perfect ramp is seen from Figure 3 to be the following:

$$f_e(t) = -\frac{\Delta f t}{\Delta T} \text{ where } |t| \le \Delta T/2 \tag{7}$$

and the corresponding phase deviation is given as follows:

$$\Delta\phi(t) = -\frac{2\pi\Delta f}{\Delta T}\frac{t^2}{2} = -\frac{\pi\Delta f t^2}{\Delta T} \quad |t| \le T/2 \tag{8}$$

which is a quadratic function. The peak–peak phase deviation is, thus, given as follows:

$$\Delta\phi_{p-p} = \Delta\phi(T/2) = \frac{\pi\Delta f(\Delta T/2)^2}{\Delta T} = \frac{\pi\Delta f\Delta T}{4} \tag{9}$$

which may be expressed in terms of the standard FMCW radar parameters, B and T, using Equation (4), as follows:

$$\Delta\phi_{p-p} = \frac{\pi\Delta f^2 T}{4B} \tag{10}$$

The Fourier series expansion of this quadratic phase modulation [10, 11] is given by the following:

$$\begin{aligned}\Delta\phi(t) &= \frac{4\Delta\phi_{p-p}}{\pi^2}\sum_{n=1}^{\infty}\frac{(-1)^2}{n^2}\cos\left(2n\pi\Delta f_{\text{sideband}}\right)\\ &= \frac{\Delta f^2 T}{\pi B}\sum_{n=1}^{\infty}\frac{(-1)^2}{n^2}\cos\left(2n\pi\Delta f_{\text{sideband}}\right)\end{aligned} \tag{11}$$

Now, assuming relatively low amplitude phase modulation, <<0.5 radians say, each phase modulation component produces a pair of sidebands in accordance with narrow-band phase modulation principles [12] with a level relative to the carrier of half the peak phase modulation, giving the final result for the amplitudes of the respective pairs of sidebands as follows:

$$\begin{aligned}&\text{sideband profile relative to target response} = \frac{\Delta f^2 T}{2\pi B n^2}\\ &= -16.0 + 20\log_{10}\left(\frac{T}{B}\right) + 40\log_{10}(\Delta f) - 40\log_{10}(n)\ \text{dBc}\\ &\text{at frequencies}: f_{\text{sideband}} = \left|\frac{2R\Delta f}{c\Delta T} \pm \frac{n}{\Delta T}\right|\end{aligned} \tag{12}$$

The finite DDS frequency increment, thus, results in a set of sidebands in the range profile around each point target at odd and even multiples of $\Delta f_{\text{sideband}}$ $(1/\Delta T)$ with amplitudes decreasing with the square of their order, n. The fundamental

pair of sidebands is dominant, with an amplitude of 12 dB above the next sideband components:

$$\text{fundamental sideband level } X = \frac{\Delta f^2 T}{2\pi B} = -16.0 + 20\log_{10}\left(\frac{T}{B}\right) + 40\log_{10}(\Delta f)\ \text{dBc} \tag{13}$$

This key result is convincingly validated in the numerical simulations of Sections 3.1 and 3.2. It is notable that the amplitudes of these DDS frequency increment-related spurious components (hereafter referred to as DDS Δf spurs) are very sensitive to the DDS frequency increment, with a $40\log_{10}$ or 40 dB/decade dependency. Equation (13) may be inverted to give a simple and convenient design equation for the required DDS frequency increment for a given peak sideband level, X,

$$\Delta f = \sqrt{\frac{2\pi BX}{T}} \tag{14}$$

For instance, if −76 dBc DDS Δf spurs are considered acceptable, then the design rule for the DDS frequency increment is given as follows:

$$\Delta f = \sqrt{\frac{B}{1000T}} \tag{15}$$

and this result may present a convenient 'rule-of-thumb', which shall be referred to as the '*−70 dBc rule*' (in view of the maximum sideband level experienced with deramp FMCW radar, as shown later). In addition to the amplitudes of these spurious components, consideration must be given to their frequencies. In some applications the DDS Δf spurs may appear outside of the radar operating range, thus allowing a more relaxed choice of DDS frequency increment, but in others may appear at ranges within the detection region of the radar where the target returns are weak and, hence, a more stringent DDS frequency increment value with lower sideband levels (X) may be necessary. The presence of DDS Δf spurs across the range profile effectively corrupts their corresponding range bins, which could be misinterpreted as false targets, particularly in the presence of weak returns.

2.2 | Deramp-based linear FMCW radar

A similar approach is now used to assess the impact of the DDS frequency increment on a linear FMCW radar based on RF deramping of the return signal using a replica chirp and mixer.

Figure 4 shows a portion of a DDS transmit chirp, at the nth and $(n + 1)$th steps, and the corresponding delayed receive chirp, as would be experienced in a linear FMCW radar system with deramp processing. The DDS frequency increment is again Δf (Hz) or $\Delta\omega$ (rad/s) and the time interval of each frequency step is again ΔT.

If the target range is such that the transmit and receive chirps are aligned by a multiple of the time interval $m\Delta T$, then after deramping, the instantaneous frequency difference will be constant with time and the instantaneous phase difference will

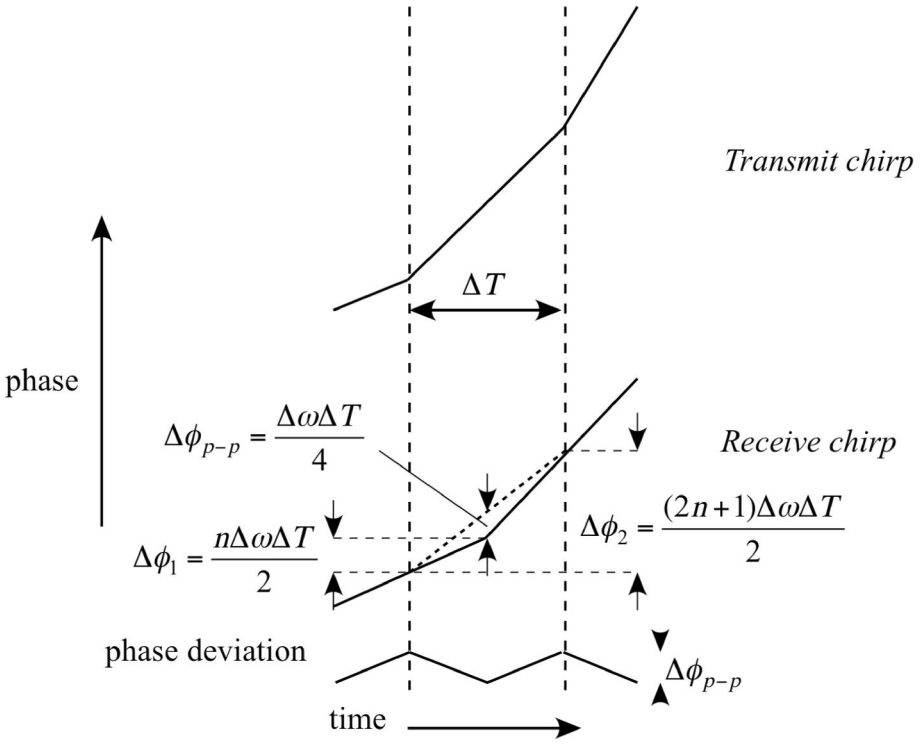

FIGURE 4 Depiction of worst-case phase deviation in a deramp FMCW radar due to the Direct Digital Synthesiser frequency increment.

be perfectly linear with time, throughout the entire radar pulse. This will result in perfect performance with no degradation due to the finite DDS frequency increment.

However, in general this will not be the case and, in particular, if the transmit and receive chirps are delayed by a multiple-plus-half of the time interval, $(m + 0.5)\ \Delta T$, then there is a clear- and worst-case triangular phase modulation of the deramped signal, with a period of ΔT. This will produce phase modulation of the deramped signal to a point target, with sidebands due to DDS frequency quantisation spaced by frequency $1/\Delta T$ as before. Figure 4 indicates this worst-case condition, from which the peak phase modulation may be derived, as follows:

The phase change of the received chirp half way through the indicated ΔT interval is given as follows:

$$\Delta\phi_1 = \frac{n\Delta\omega\Delta T}{2} \tag{16}$$

and the phase change at the end of the same ΔT interval is given as follows:

$$\Delta\phi_2 = \frac{n\Delta\omega\Delta T}{2} + \frac{(n+1)\Delta\omega\Delta T}{2} = \frac{(2n+1)\Delta\omega\Delta T}{2} \tag{17}$$

The phase mid-way along the mean phase trajectory, shown by the dashed diagonal, is, thus, given as follows:

$$\frac{\Delta\phi_2}{2} = \frac{(2n+1)\Delta\omega\Delta T}{4} \tag{18}$$

and so the peak–peak phase deviation from the steady linear phase trajectory, in the middle of the ΔT interval, is given as follows:

$$\Delta\phi_{p-p} = \frac{(2n+1)\Delta\omega\Delta T}{4} - \frac{n\Delta\omega\Delta T}{2} = \frac{\pi\Delta f\Delta T}{2} \tag{19}$$

which may be expressed in terms of the standard FMCW radar parameters, B and T, using Equation (4), as given below:

$$\Delta\phi_{p-p} = \frac{\pi\Delta f^2 T}{2B} \tag{20}$$

The Fourier series expansion of this triangular phase modulation [10, 11] is given by the following:

$$\begin{aligned}\Delta\phi(t) &= \frac{4\Delta\phi_{p-p}}{\pi^2}\sum_{n=1}^{\infty}\frac{(-1)^2}{(2n-1)^2}\sin\left[(2n+1)2\pi\Delta f_{\text{sideband}}\right] \\ &= \frac{2\Delta f^2 T}{\pi B}\sum_{n=1}^{\infty}\frac{(-1)^2}{(2n-1)^2}\sin\left[(2n+1)2\pi\Delta f_{\text{sideband}}\right]\end{aligned} \tag{21}$$

Again assuming relatively low amplitude phase modulation, <<0.5 radians say, each phase modulation component will produce a pair of sidebands in accordance with narrow-band phase modulation principles [12] with a level relative to the carrier of half the peak phase modulation, giving the final result for the amplitudes of the respective pairs of sidebands:

$$\text{sideband profile relative to target response} = \frac{\Delta f^2 T}{\pi B(2n-1)^2} \tag{22}$$

The worst-case DDS Δf spurs are, thus, twice the amplitude of those obtained with direct sampling processing; however, there are now only odd sidebands, and the fundamental pair of spurs have an amplitude 19 dB greater than the next order sidebands, as given by the following:

$$\text{fundamental sideband level } X = \frac{\Delta f^2 T}{\pi B} = -9.9 + 20\log_{10}(T/B) + 40\log_{10}(\Delta f)\ \text{dBc} \tag{23}$$

This key result is convincingly validated in the numerical simulations of Sections 3.3 and 3.4. As before, the expression may be inverted to give a simple and convenient design equation for the required DDS frequency increment for a given peak sideband level relative to carrier, X,

$$\Delta f = \sqrt{\frac{\pi BX}{T}} \tag{24}$$

For instance, if −70 dBc DDS Δf spurs are considered acceptable, then the design rule for the DDS frequency increment is again,

$$\Delta f = \sqrt{\frac{B}{1000T}} \tag{25}$$

3 | NUMERICAL SIMULATION OF THE IMPACT OF DDS FREQUENCY INCREMENT ON DIRECT-SAMPLING AND DERAMP LINEAR FMCW SYSTEMS

Validation of the analytic theory and key results presented in Section 2 has been performed by means of a numerical simulation of the two types of FMCW radar system. The simulations involve generation of a step-frequency approximation to a transmit chirp and processing with either delayed versions of a perfect continuous chirp, for the direct sampling architecture, or a delayed version of the transmitted, step-frequency chirp, for the deramp architecture. The simulations are performed to a high temporal resolution, with 10 million samples to represent a single radar pulse.

The absolute B and T parameters chosen for the numerical simulation are somewhat arbitrary as the Δf spur distribution is related to the B/T value (Equations (12) and (22)), but the numerical simulation shown here is based on a real radar system being developed at UCL to image volcano flows. In this system, an Analogue Devices AD9914 DDS [13] is employed and configured for 1 GHz sweep bandwidth and 10 ms pulse duration. The desired maximum operating range in this application is 5 km and the desired range resolution is around 15 cm.

3.1 | Direct sampling processing, 100 kHz DDS increment

Figure 5 shows the numerically-modelled phase deviation for this radar, after direct sampling processing with a perfect continuous chirp, at a range of 2930 m with a 100 kHz DDS frequency increment. This is equivalent to 10 times the *−70 dBc rule* frequency increment of $\sqrt{(B/1000T)}$, Equation (15).

The phase modulation is parabolic with a peak–peak value of 78.54 mrads. The analytically predicted phase deviation from Equation (10) is 78.54 mrads, so they are in perfect agreement. The frequency of the modulation is 1 MHz, as expected from Equation (5).

The modelled range profile, in Figure 6, contains pairs of sidebands spaced by 1 MHz or 1.5 km in range, as expected from Equations (5) and (6). Some of these sidebands are of a negative frequency and so are foldover in the spectrum. If complex (IQ) processing is employed then these negative frequencies will instead remain as negative frequencies, without foldover.

Both odd and even sidebands are present, as expected. The modelled amplitudes of the first, second and third sidebands are −35.96, −48.00 and −55.05 dBc, respectively. By comparison, the analytically-predicted amplitudes, from Equation (12), are −35.96, −48.00 and −55.05 dBc, in perfect agreement.

It is clear that, in this application, a 100 kHz DDS increment produces high sidebands (c. −36 dBc) within the intended operating range of the instrument and so this choice of DDS frequency increment is inappropriate.

3.2 | Direct sampling processing, 10 kHz DDS increment

The design formula, $\sqrt{(B/1000T)}$, Equation (15), suggests a DDS increment of 10 kHz for this radar for −76 dBc sidebands. Figure 7 shows the numerically-modelled phase deviation due to DDS increment of this radar, after direct sampling processing, at the same range of 2930 m, but now with 10 kHz frequency increment. The phase modulation is again parabolic but now with a peak–peak value of 0.785 mrads, the same as the predicted phase modulation from Equation (10). This is 100 times lower than before due to the square-law dependence on the frequency increment. The frequency of the modulation is now 10 MHz, as per Equation (5).

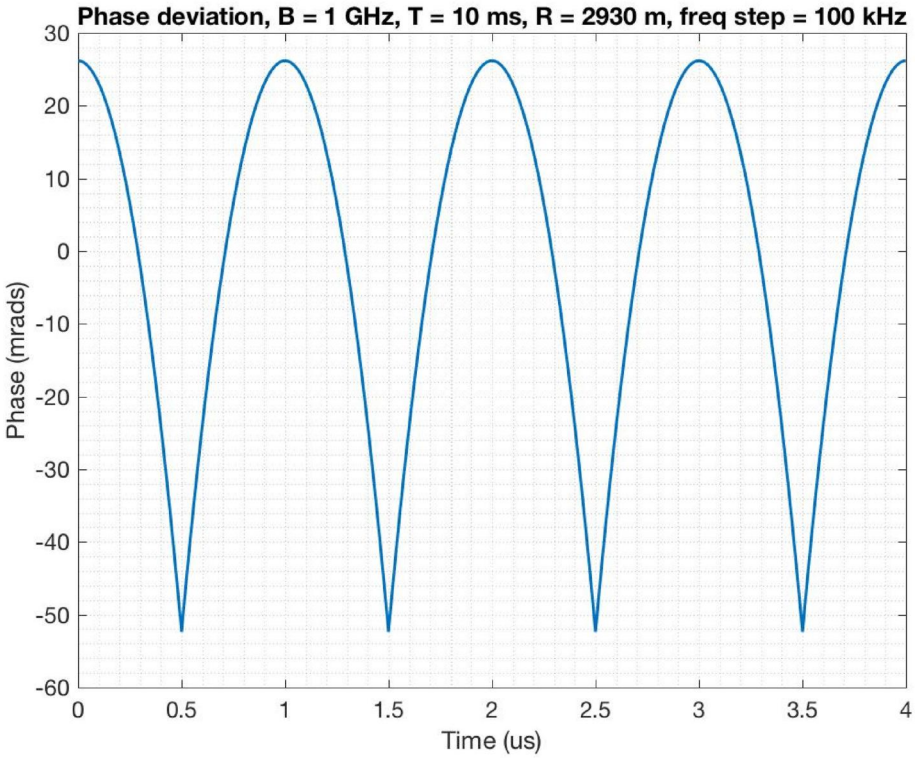

FIGURE 5 Numerically-modelled phase deviation of a direct-sampling linear FMCW radar, with 100 kHz Direct Digital Synthesiser frequency increment, 1 GHz sweep bandwidth and 10 ms pulse duration.

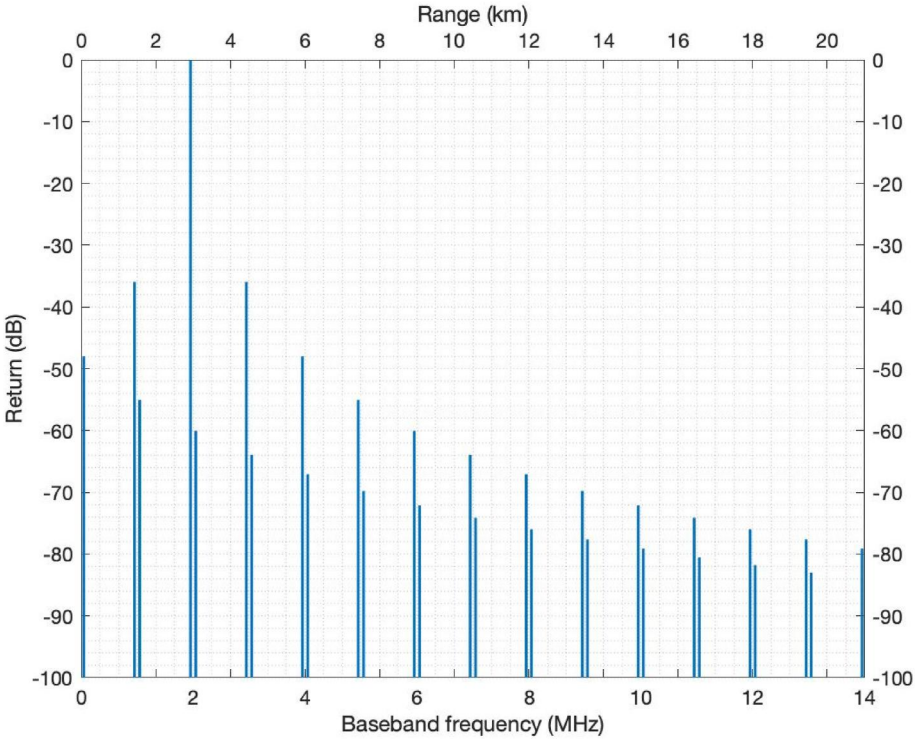

FIGURE 6 Numerically-modelled range profile obtained with a direct sampling FMCW radar, with 100 kHz DDS frequency increment, 1 GHz sweep bandwidth and 10 ms pulse duration. Ten times the *−70 dBc rule* DDS frequency increment. DDS, Direct Digital Synthesiser.

The modelled range profile, in Figure 8, contains a single pair of sidebands spaced by 10 MHz or 15 km in range, as expected from Equations (5) and (6). The sidebands are at approximately 2 ± 10 MHz, where the negative frequency sideband foldsover to 8 MHz. The modelled sideband amplitude is −75.96 dBc, exactly 40 dB lower than with a 100 kHz DDS increment, as expected from the 40 dB/decade behaviour. The analytically-predicted sideband amplitude, from Equation (12), is −75.96 dBc, in perfect agreement with the model.

3.3 | Deramp processing, 100 kHz DDS increment

Again, the modelling starts with a frequency increment 10 times the *−70 dBc rule* of $\sqrt{(B/1000T)}$, Equation (25). Figure 9 shows the numerically-modelled phase deviation of this radar, after deramp processing, at a range of 2925 m with a 100 kHz DDS frequency increment. The range is chosen here for a round-trip delay of 19.5 times the DDS time increment, in order to produce a worst-case result, as explained in Section 2.2. The phase modulation is now triangular and with a peak–peak value of 157.1 mrads. The analytically-predicted phase modulation from Equation (20) is 157.1 mrads, in perfect agreement with the modelling. The frequency of the modulation is 1 MHz, as expected from Equation (5).

The modelled range profile, in Figure 10, contains pairs of sidebands spaced by 1 MHz or 1.5 km in range, as expected from Equations (5) and (6). Some of these sidebands are of a negative frequency and so foldover in the spectrum. Again, if complex (IQ) deramping is employed then these negative frequencies will instead remain as negative frequencies, without foldover, although deramp radars rarely use IQ processing in order to reduce costs.

The sidebands are predominantly odd, but some even order sidebands are also visible at a lower level. This may be due to intermodulation between the first pair of sidebands and the carrier, due to the phase modulation being of sufficient depth to exhibit a certain amount of non-linearity. The modelled amplitudes of the first, third and fifth sidebands are −29.95, −49.05 and −57.93 dBc, respectively. The analytically-predicted amplitudes, from Equation (22), are −29.94, −49.03 and −57.90 dBc, in excellent agreement, to within 0.03 dB. The amplitudes of the highest sidebands are 6.01 dB higher with deramp processing than direct sampling, as expected from theory.

It is clear that, in this application, a 100 kHz DDS increment produces high sidebands (c. −30 dBc) within the intended operating range of the instrument and so this choice of DDS frequency increment is inappropriate.

3.4 | Deramp processing, 10 kHz DDS increment

The design formula, $\sqrt{(B/1000T)}$, Equation (25), suggests a DDS increment of 10 kHz for this radar for −70 dBc spurious

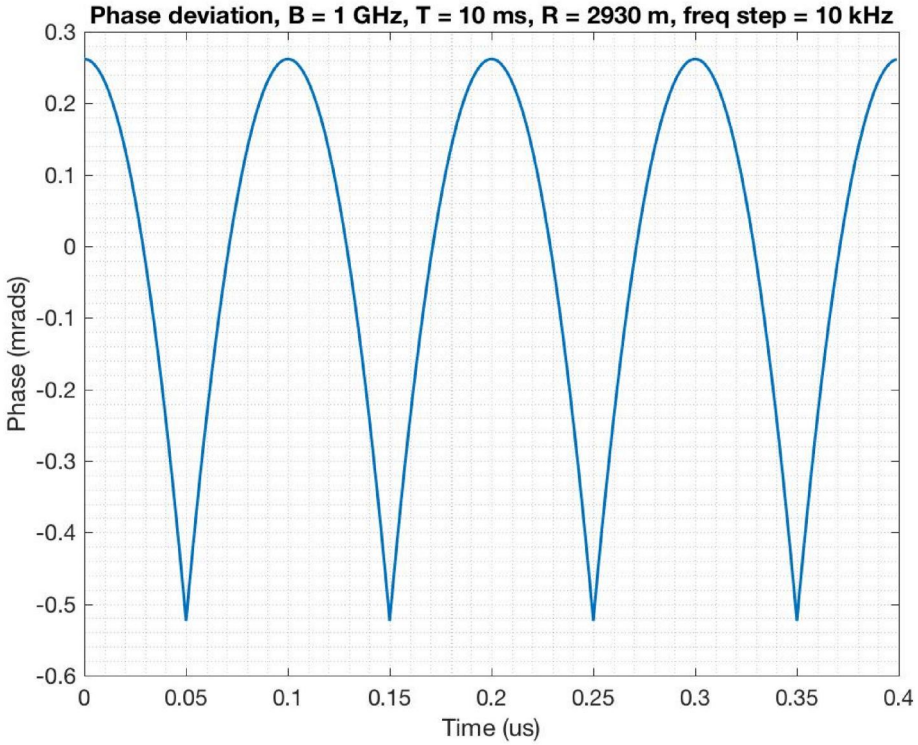

FIGURE 7 Numerically-modelled phase deviation of a direct sampling FMCW radar, with 10 kHz Direct Digital Synthesiser frequency increment, 1 GHz sweep bandwidth and 10 ms pulse duration.

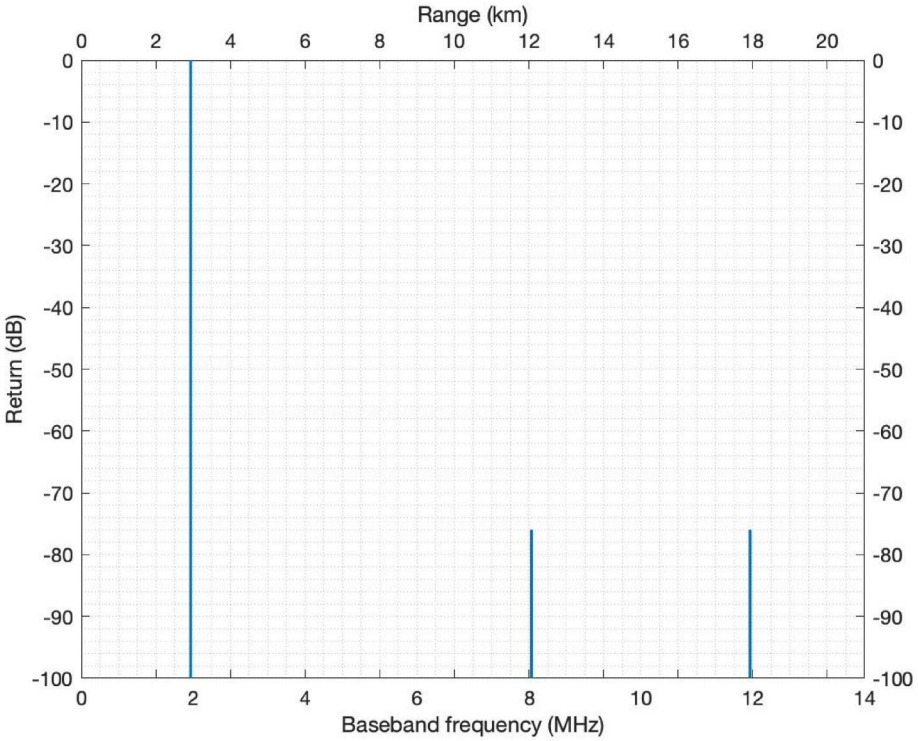

FIGURE 8 Numerically-modelled range profile obtained with a direct sampling FMCW radar, with 10 kHz Direct Digital Synthesiser frequency increment, 1 GHz sweep bandwidth and 10 ms pulse duration. The *−70 dBc rule* frequency increment.

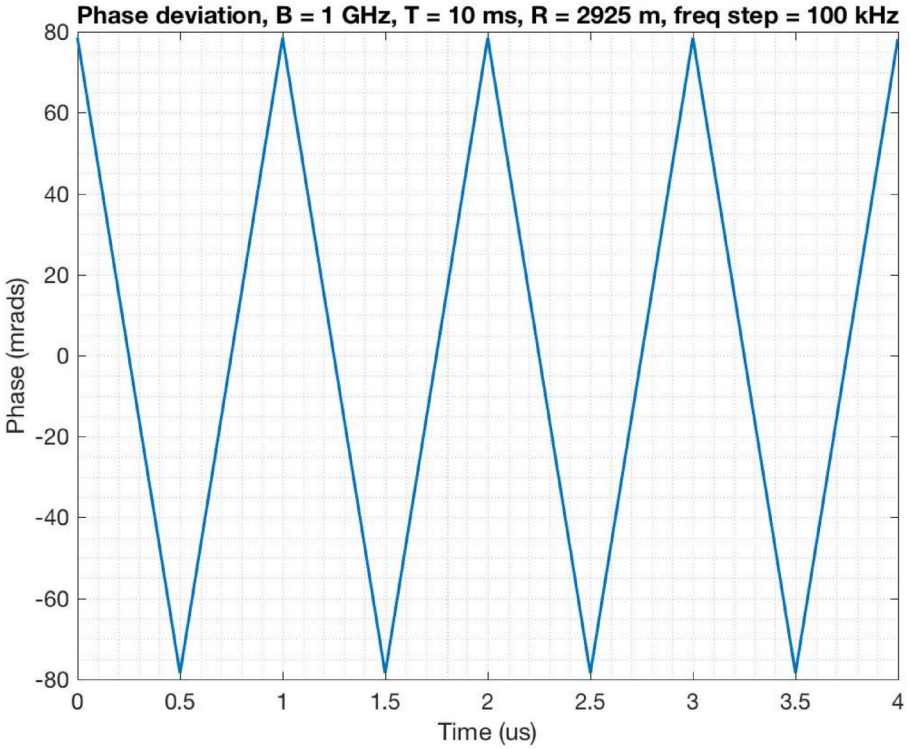

FIGURE 9 Numerically-modelled phase deviation of a deramp FMCW radar, with 100 kHz Direct Digital Synthesiser frequency increment, 1 GHz sweep bandwidth and 10 ms pulse duration.

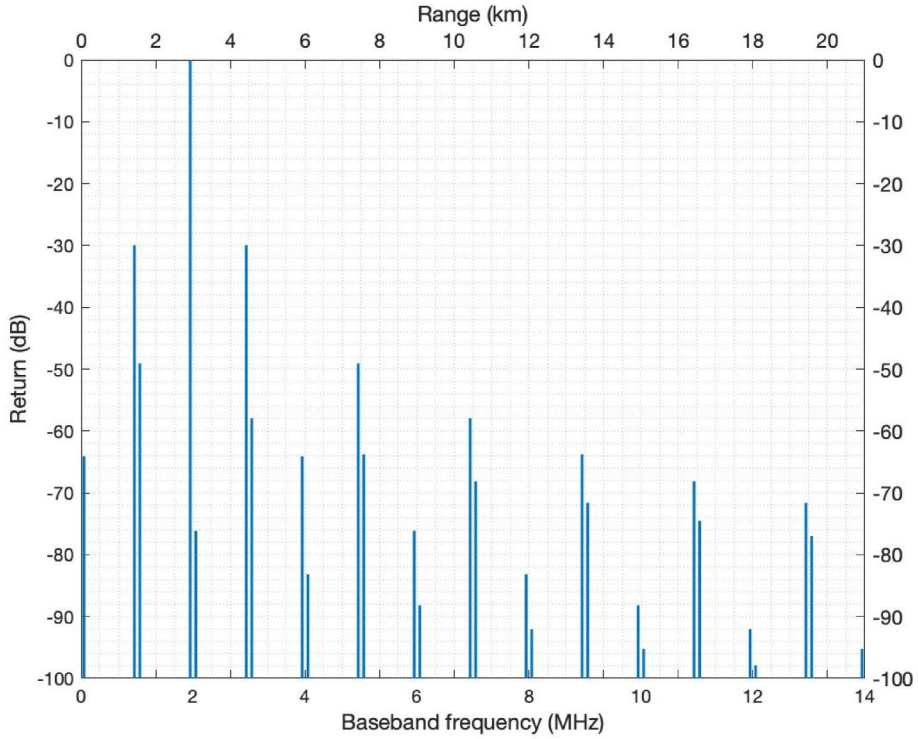

FIGURE 10 Numerically-modelled range profile obtained with a deramp linear FMCW radar, with 100 kHz DDS frequency increment, 1 GHz sweep bandwidth and 10 ms pulse duration. Ten times the *−70 dBc rule* DDS frequency increment. DDS, Direct Digital Synthesiser.

sidebands. Figure 11 shows the numerically-modelled phase deviation of this radar, after deramp processing, at a similar range of 2932.5 m but now with a 10 kHz DDS increment. The range is chosen here for a round-trip delay of 195.5 times the DDS time increment, in order to produce a worst-case result, as explained in Section 2.2. The phase modulation is again triangular but now with a peak–peak value of 1.571 mrads, the same as the analytically-predicted phase modulation from Equation (20). The frequency of the modulation is now 10 MHz, as per Equation (5).

The modelled range profile, in Figure 12, contains a single pair of sidebands spaced by 10 MHz or 15 km in range, as expected from Equations (5) and (6). The sidebands are at approximately 2 ± 10 MHz, where the negative frequency sideband folds over to 8 MHz. The modelled sideband amplitude is −69.94 dBc. The analytically-predicted sideband amplitude, from Equation (22), is −69.94 dBc, in perfect agreement.

Since the sideband spacing is 10 MHz or 15 km then these spurious sidebands will not be visible in this application within the desired operating range of 5 km, this choice of frequency increment is suitable for this radar system and application. A smaller increment may also be suitable, but is unnecessary.

It should be noted that, since these spurious components arise due to phase modulation, then windowing prior to taking the FFT will have no effect, in contrast to the usual case of range sidelobes that may benefit from windowing. Hence, the deliberate use of the term *range sidebands* in this paper.

In this particular example, the DDS Δf spurs spacing is 10 MHz,or 15 km, and so these range sidebands will not be an issue application due to the desired maximum operating range of 5 km. Hence, a higher DDS frequency increment may be suitable for this radar system. Indeed, in general, the closest and largest Δf spur will be outside of the maximum operating range, $R_{\max}$, of the radar if the following is satisfied:

$$\Delta R_{\text{sideband}} > \frac{R_{\max}}{2} \Rightarrow \Delta f < \frac{c}{4R_{\max}} \tag{26}$$

For the example considered here the requirement for DDS Δf spurs to fall beyond the maximum operating range is, thus, $\Delta f < 15$ kHz, so a slight relaxation in the DDS frequency increment is possible. As a more extreme example, an ice-sounding radar system [14] developed by UCL and BAS uses a 200 MHz sweep bandwidth and 1 s pulse duration, with a maximum operating range (air equivalent) of around 5000 m. This requires, for the −70 dBc spur rule to be satisfied, $\Delta f < 447$ Hz, but for the out-of-range spur condition to be satisfied, $\Delta f < 15$ kHz; hence, a design value approaching 15 kHz would be acceptable. This example, however, is not typical in view of the very long pulse duration and there may be other intermodulation issues with the use of a large frequency step that is known to produce high, though out-of-band, spurs, so prudence may still favour the *−70 dBc rule*.

3.5 | Multiple targets and noise/clutter

A more realistic impression of performance may be obtained with multiple targets and in the presence of noise. Figures 13

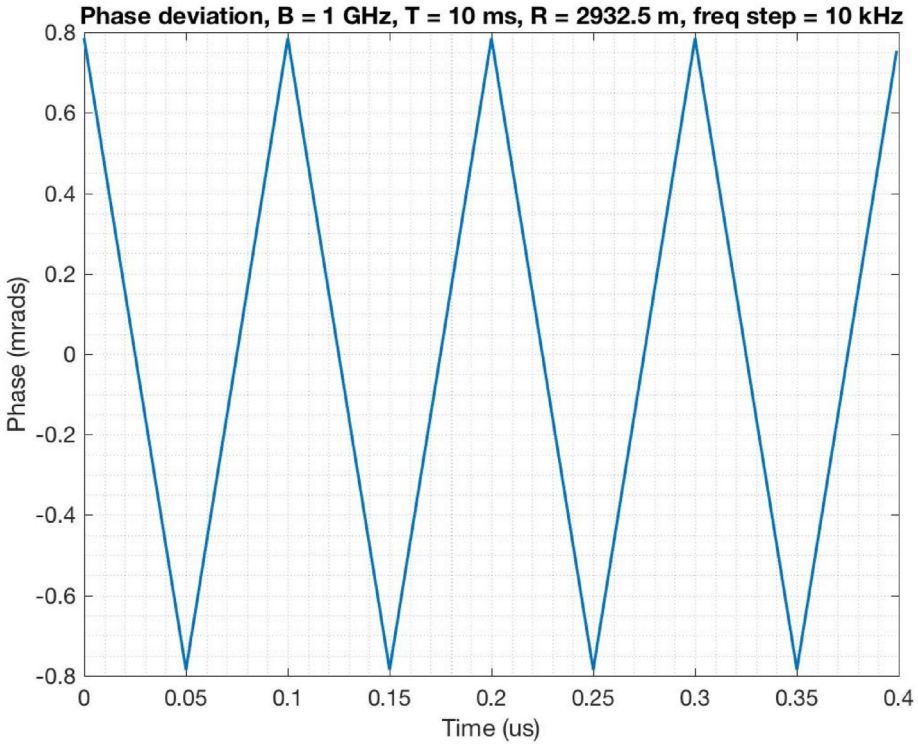

FIGURE 11 Numerically-modelled phase deviation of a deramp FMCW radar, with 10 kHz Direct Digital Synthesiser frequency increment, 1 GHz sweep bandwidth and 10 ms pulse duration.

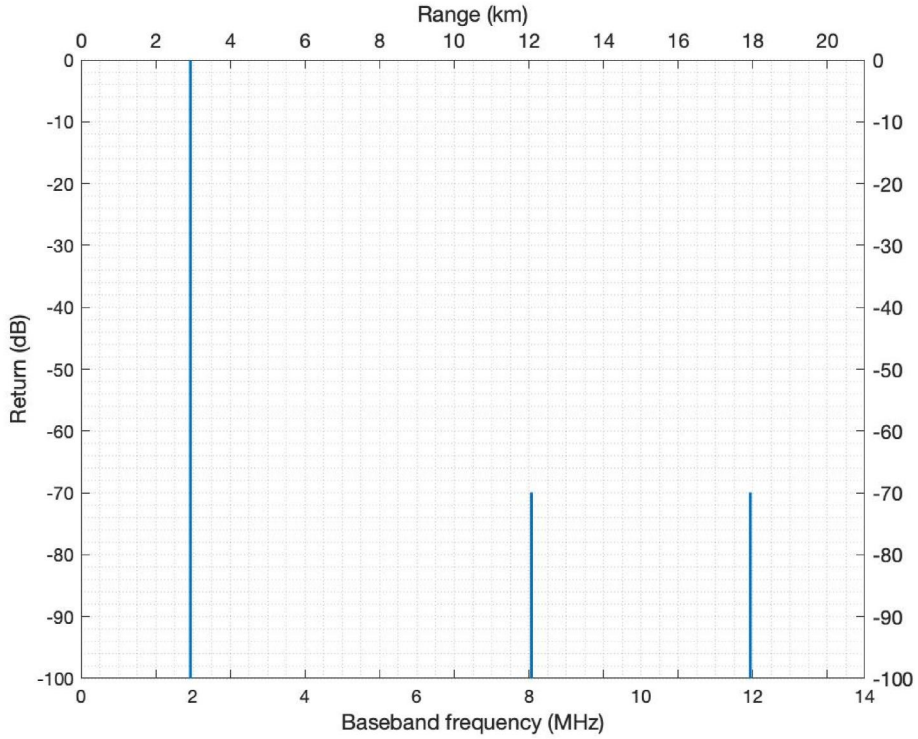

FIGURE 12 Numerically-modelled range profile obtained with a deramp FMCW radar, with 10 kHz DDS frequency increment, 1 GHz sweep bandwidth and 10 ms pulse duration. The *−70 dBc rule* DDS frequency increment. DDS, Direct Digital Synthesiser.

and 14 are results of a numerical simulation of a strong target at 1.2 km range and a 40 dB weaker target at 4 km range, in the presence of noise of approximately −70 dBc in the $1/T$ detection bandwidth. The direct sampling architecture is modelled with the same radar parameters as before.

In Figure 13, the DDS increment is set to 100 kHz. The range profile is more complicated with a richer set of spurious components. The 1.2 km, 0 dB target is clearly visible and the 4 km, −40 dB target is visible but surrounded by a number of spurious components due to the large DDS increment. Some 10 spurious components are apparent, two of which are stronger than the 4 km target, which somewhat obscure this target.

In Figure 14, the DDS increment is set to 10 kHz (the *−70 dBc rule*). Both targets are now clearly visible and there are no discernible spurious components.

Of course, a realistic situation will comprise numerous targets, clutter and other sources of reflected signal, and so an inappropriate choice of DDS frequency increment may lead to many spurious components due to the mechanism outlined in this paper.

4 | EXPERIMENTAL RESULTS

4.1 | Direct sampling FMCW radar

Experimental validation has been performed using an FMCW signal generated from an Analog Devices AD9910 DDS [15] programed with 20 MHz sweep bandwidth (20–40 MHz) and 10 ms pulse duration. The DDS was externally driven by a 10 MHz crystal oscillator and the internal PLL was activated to operate the DDS at a clock rate of 1 GHz. The FMCW signal was directly sampled at 100 MSa/s using a digital oscilloscope and then processed offline by multiplying with a replica chirp and taking the FFT to achieve pulse compression. The replica chirp was delayed by 250 μs, equivalent to a 500 kHz baseband frequency corresponding to a target at 37.5 km range.

The analytically-predicted peak sideband level is given by the following, from Equation (12):

$$\text{fundamental spur amplitude} = \frac{\Delta f^2 T}{2\pi B} \tag{27}$$

where T and B are constant in this set of measurements as would be the case in a typical radar application. The frequencies of the fundamental pair of sidebands are equal to the target frequency $\pm 1/\Delta T$:

$$f_{\text{sideband}} = \left| \frac{2R\Delta f}{c\Delta T} + \frac{1}{\Delta T} \right| \tag{28}$$

where the modulus function represents spectrum foldover of any negative frequencies.

Five values of frequency increment were chosen, with the DDS parameters, analytically-predicted results and experimentally-measured results as summarised in Table 1.

Plots of the spectra obtained with these five sets of parameters are shown in Figure 15, where plots (d) and (e) exhibit spectrum foldover. The predicted positions of the fundamental

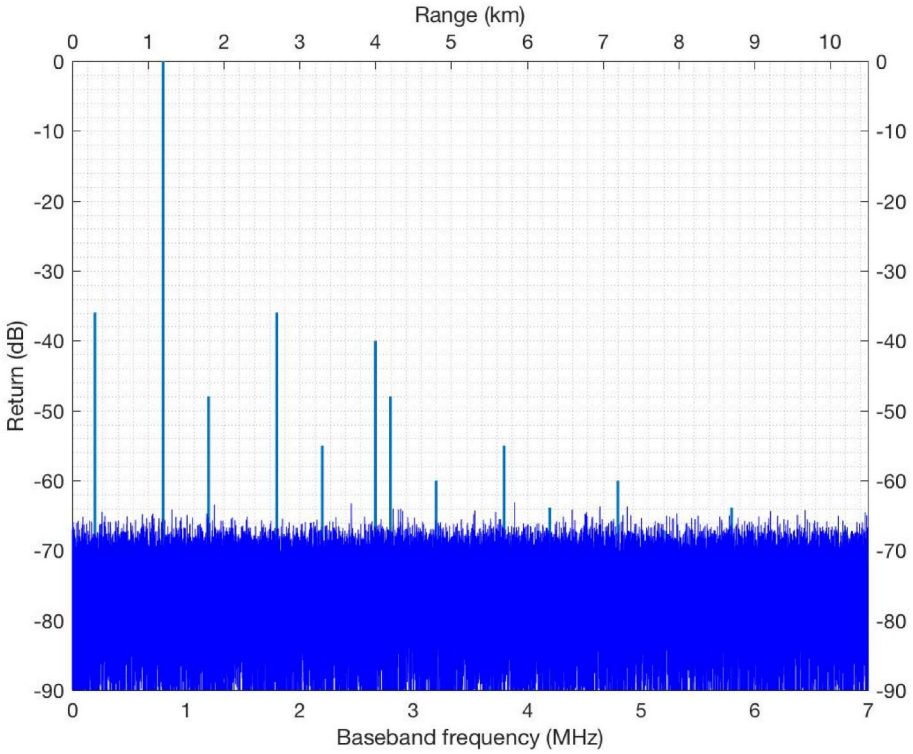

FIGURE 13 Numerically-modelled range profile, direct sampling FMCW radar, two targets with 100 kHz DDS frequency increment, 1 GHz sweep bandwidth and 10 ms pulse duration. Ten times the *−70 dBc rule* DDS frequency increment. DDS, Direct Digital Synthesiser.

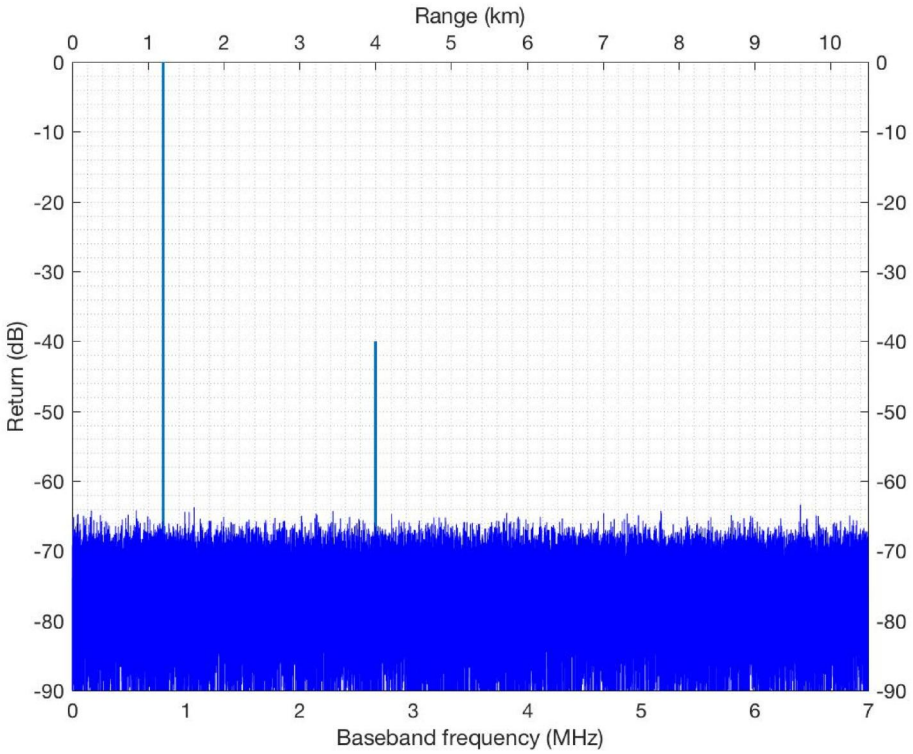

FIGURE 14 Numerically-modelled range profile, direct sampling FMCW radar, two targets with 10 kHz DDS frequency increment, 1 GHz sweep bandwidth and 10 ms pulse duration. The *−70 dBc rule* DDS frequency increment. DDS, Direct Digital Synthesiser.

TABLE 1 Parameters used for experimental validation with a direct-sampling FMCW radar.

DDS time increment, ΔT(μs)	**7.056**	**3.968**	**2.232**	**1.256**	**0.7040**
DDS frequency increment, Δf(Hz)	14,113.03	7936.03	4462.9	2509.91	1410.95
Sweep bandwidth, B (MHz)	20	20	20	20	20
Pulse duration, T (ms)	10	10	10	10	10
Predicted sideband frequencies (kHz) (for 500 kHz target)	358.3	248.0	52.7	296.8	917.2
	641.7	752.0	948.3	1296.8	1917.2
Predicted max sideband level (dBc)	−36.0	−46.0	−56.0	−66.0	−76.0
Measured max sideband level (dBc)	−36.0	−45.7	−55.5	−62.8	−69.9
	−36.0	−45.4	−55.1	−64.5	−71.1

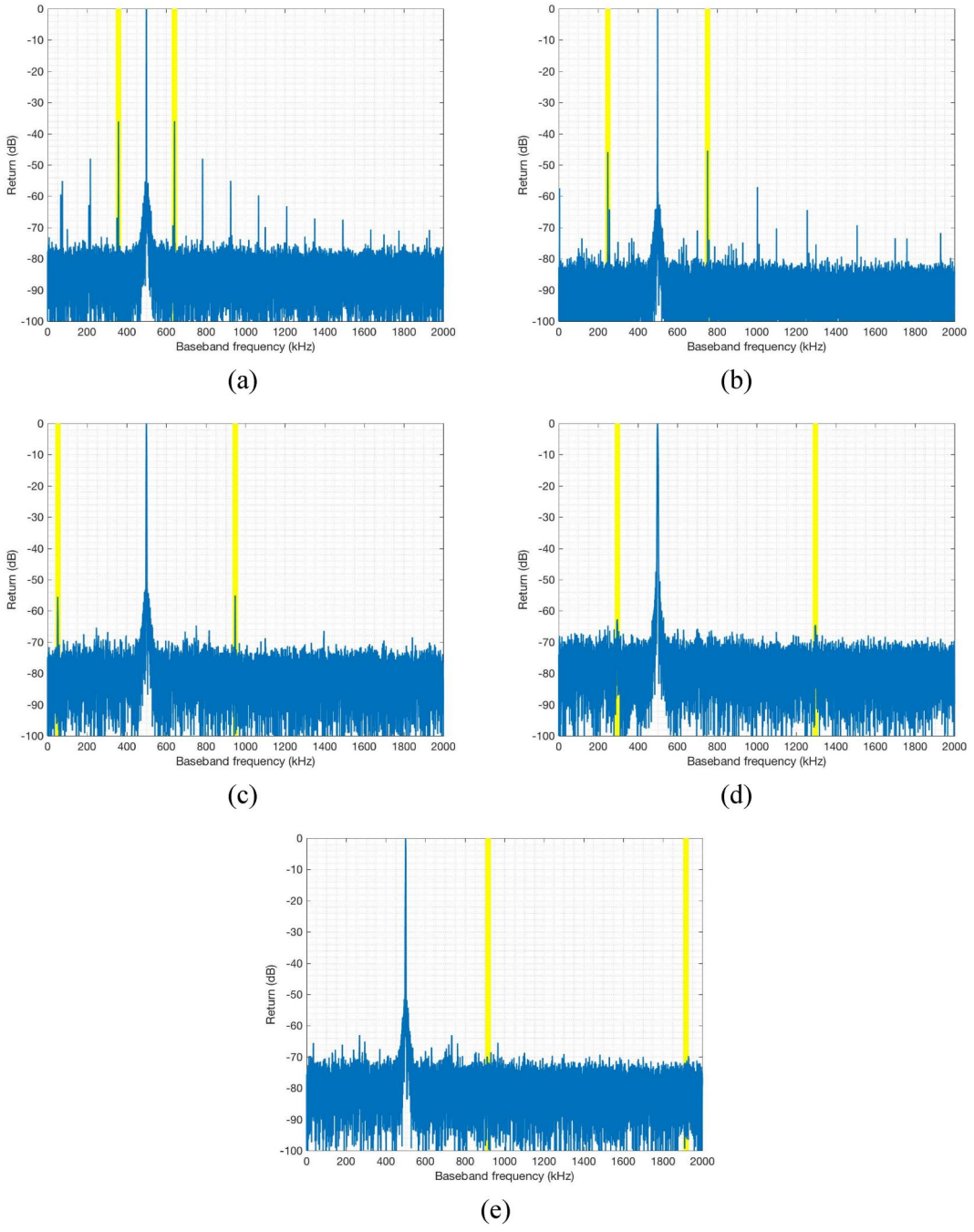

FIGURE 15 Measured Direct Digital Synthesiser Δf spurs, direct sampling, for predicted fundamental spur levels of −36 dBc (a) to −76 dBc (e).

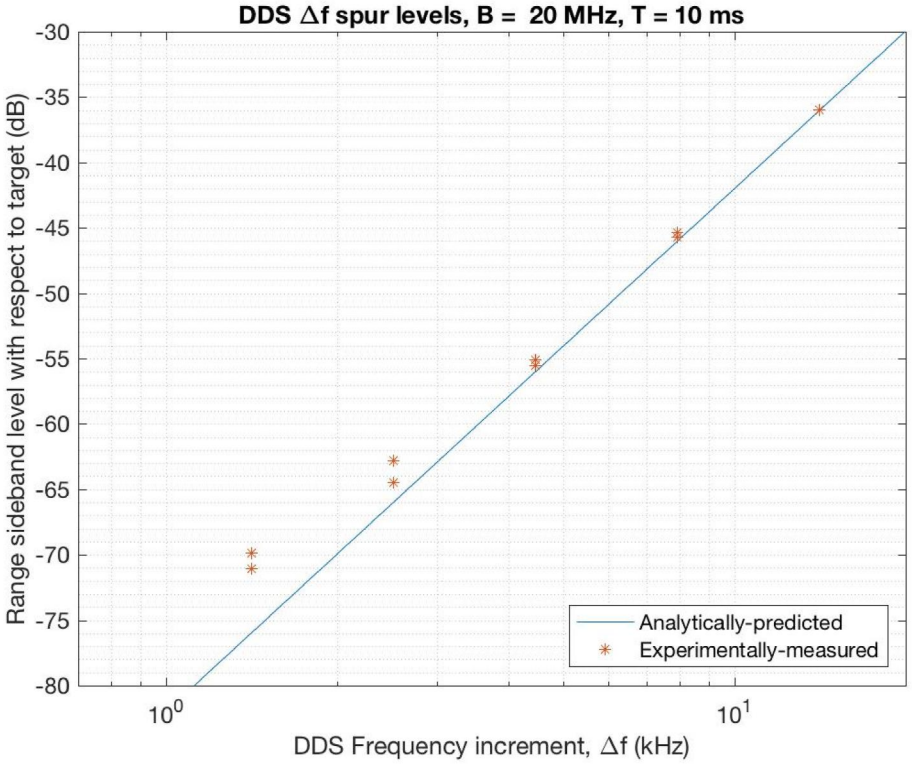

FIGURE 16 Summary of experimentally-measured versus analytically-predicted Direct Digital Synthesiser Δf spurs with a deramp FMCW radar, with constant B and T values.

DDS Δf spur order, n	1	2	3	4	5	6
Analytically-predicted spur level (dBc)	−36.0	−48.0	−55.1	−60.1	−64.0	−67.1
Measured spur level (dBc)	−36.0	−47.9	−55.1	−59.7	−63.2	−67.1

Abbreviation: DDS, Direct Digital Synthesiser.

TABLE 2 Analytically-predicted versus measured DDS Δf spur distribution.

DDS Δf spurs are indicated by the yellow vertical bands. The spurs are readily visible in four of the plots (−36 to −66 dBc) at the predicted frequencies. The noise floors vary from approximately −70 to −80 dBc and make it difficult to identify the −76 dBc spurs.

The fundamental DDS Δf spur levels indicated in these plots are summarised in Figure 16 alongside the analytically-predicted values, from Equation (27). There is good general agreement in the results, to within 1 dB for the higher spur levels of −36 to −56 dBc. For the lower spur levels of −66 and −76 dBc, the measured spurs are some 3 and 5 dB higher than predicted, most likely due to the finite noise floor. Spur levels increase with Δf at a rate of 40 dB/decade, as expected from Equation (27). It is noticeable that there are various additional spurs in the baseband spectrum due to other aspects of DDS behaviour, probably resulting from circuit imperfections and intermodulation. Hence, a DDS Δf spur level of −76 dBc would seem quite sufficient to ensure good performance within the context of other noise and clutter in a real system.

The DDS Δf spur distribution is clearly visible in the first two of these plots. Table 2 shows the measured versus analytically-predicted spur levels of the different orders of spur for −36 dBc fundamental sideband levels (Figure 15a). The predicted values can be found in Equation (12). There is excellent correspondence between measurement and analytic theory, and within 0.3 dB means absolute error.

4.2 | Deramp FMCW radar

Experimental validation has been performed using an Analog Devices AD9910 DDS [15], but this time operated with a 200 MHz sweep bandwidth and a 250 m cable loop to create a time delay equivalent to a single target. Initial measurements established that the electrical length, L, of the path is 380 m, with a corresponding time delay of 1.26 μs. In order to produce the worst-case sideband levels (from Figure 4), the DDS time increment, ΔT, was set to twice this value, 2.532 μs, and the DDS frequency increment, Δf, was set for the required sideband level as obtained analytically in Section 2.2.

The analytically-predicted peak sideband level is found from a variation of Equation (22):

TABLE 3 Parameters used for experimental validation with a deramp FMCW radar.

DDS time increment, ΔT(μs)	**2.532**	**2.532**	**2.532**	**2.532**	**2.532**
DDS frequency increment, Δf(Hz)	39,215	12,401	3922	1240	392.1
Sweep bandwidth, B (MHz)	200	200	200	200	200
Pulse duration, T (ms)	13	41	129	408	12,901
Predicted sideband frequencies (kHz)	375.3	388.7	393.0	394.3	394.8
	414.6	401.1	396.9	395.6	395.2
Predicted max sideband level (dBc)	−30.0	−40.0	−50.0	−60.0	−70.0
Measured max sideband level (dBc)	−30.8	−40.7	−51.0,	−58.3	−65.1
	−30.7	−40.1	−50.8	−57.2	−64.2

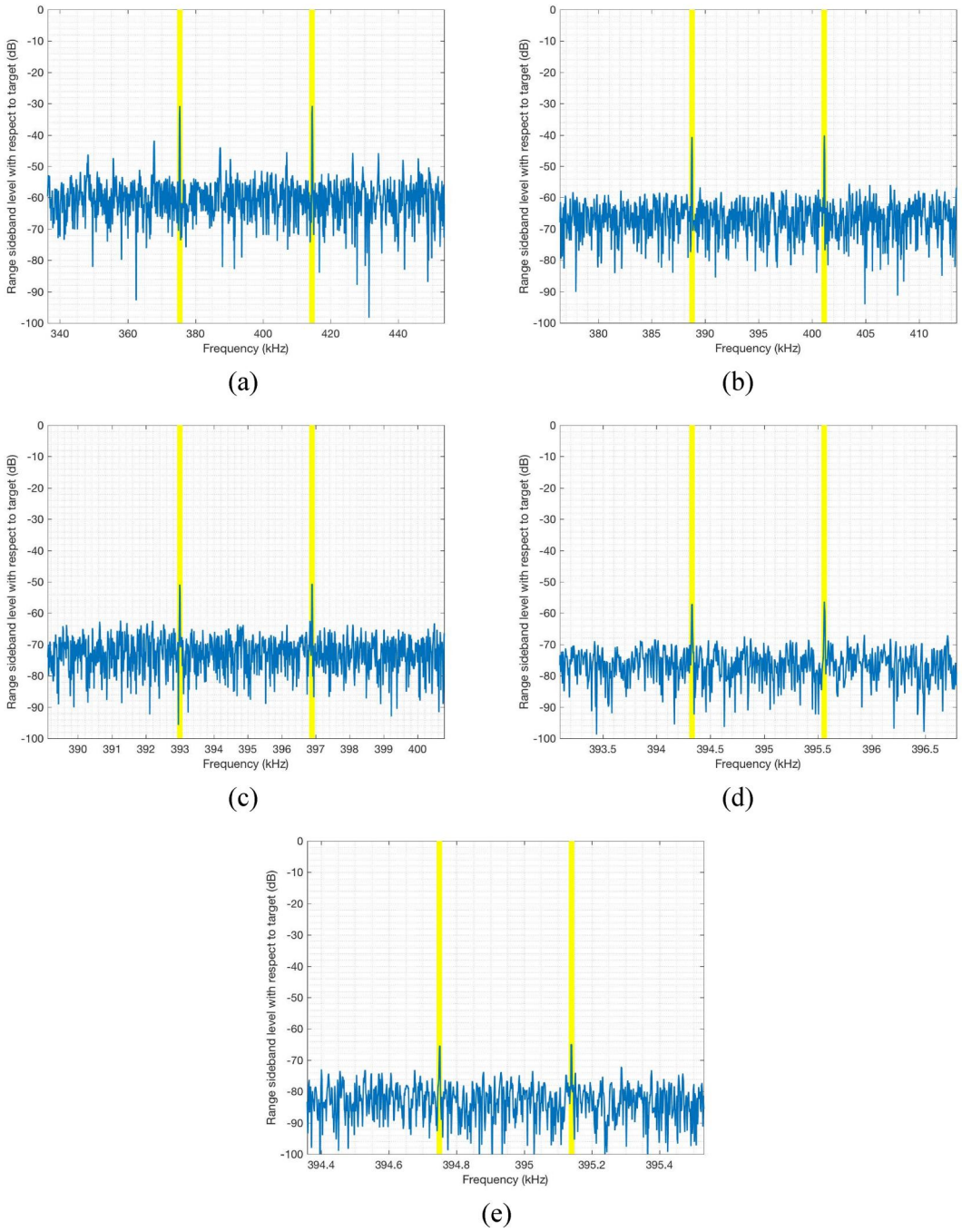

FIGURE 17 Measured Direct Digital Synthesiser Δf spurs for predicted spur levels of −30 dBc (a) to −70 dBc (e).

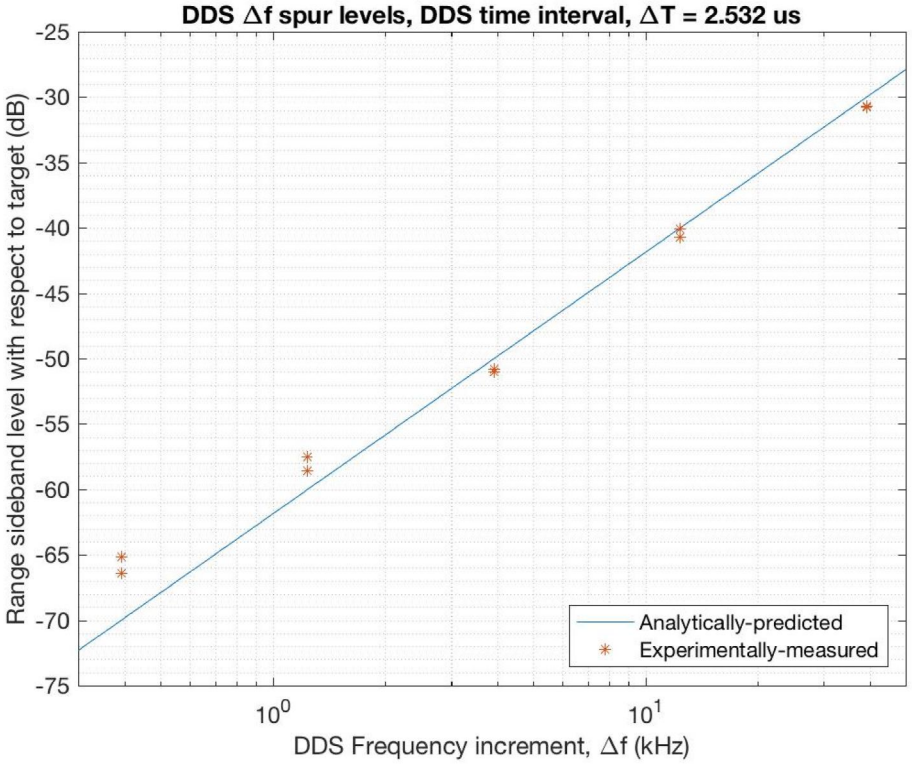

FIGURE 18 Summary of experimentally-measured versus analytically-predicted Direct Digital Synthesiser Δf spurs with a deramp FMCW radar, ΔT held constant.

$$\text{fundamental spur amplitude} = \frac{\Delta f^2 T}{\pi B} \equiv \frac{\Delta f \Delta T}{\Delta T} \tag{29}$$

where ΔT is constant in this set of measurements in order to maintain a round-trip delay of one half of the DDS time increment. The frequencies of the fundamental pair of sidebands are again equal to the target frequency $\pm 1/\Delta T$:

$$f_{\text{sideband}} = \left| \frac{\Delta f L}{c \Delta T} + \frac{1}{\Delta T} \right| \tag{30}$$

Five values of frequency increment were chosen, with the DDS parameters, analytically-predicted results and experimentally-measured results as summarised in Table 3.

Plots of the spectra obtained with these five sets of parameters are shown in Figure 17. Because of the radar parameters used in this measurement, the plots are zoomed in to clearly show the DDS Δf spurs, the predicted positions of which are again indicated by the yellow vertical bands. The spurs are readily visible in all five plots exactly at the predicted frequencies. The noise floors vary from approximately −60 to −80 dBc due to the increasing pulse durations and, hence, sample length over the measurements.

The sideband levels indicated in these plots are summarised in Figure 18 alongside the analytically-predicted values, from Equation (29). There is good general agreement in the resultswithin 1 dB for the higher spur levels of −30 to −50 dBc. For the lower spur levels of −60 and −70 dBc, the measured spurs are some 2 and 4 dB higher than predicted, which is probably due to system imperfections such as nonlinearities and the finite noise floor. In contrast with the direct sampling results, spur levels increase with Δf at a rate of 20 dB/decade, as expected from Equation (29), due to the need to maintain a constant DDS time increment. This result tends to justify −70 dBc as a sensible design criterion for DDS Δf spur level in view of real-world artefacts of noise, nonlinearities and clutter, which are likely to have a greater impact.

The measured results, as a whole, are very pleasing and convincingly validate the theory developed in this paper and justify the proposed $\sqrt{(B/1000T)}$ (*−70 dBc rule*) for the choice of DDS frequency increment, Δf.

5 | CONCLUSIONS

The purpose of this paper is to provide an insight into the impact of and appropriate choice of frequency increment for DDS-based linear FMCW radar system design.

It is shown that the finite frequency increment in a DDS-based linear FMCW radar results in phase modulation of the direct sampling/deramped FMCW signal, and a particular set of spurious range sidebands that may adversely impact performance. Analysis presented here has led to a simple set of analytic results relating the amplitudes and frequencies of these DDS Δf spurs to the DDS frequency increment and the basic radar parameters of sweep bandwidth and pulse duration,

taking into account the maximum target detection range. It is shown that the amplitudes of these spurs increase with the square of the DDS frequency increment, and have a slightly different distribution and level depending on whether direct sampling or deramp FMCW radar is used.

The analysis is convincingly validated by numerical simulation of both direct sampling/SDR and deramp FMCW radar architectures. All analytic results are shown to correspond precisely with simulation. Measurements with a direct sampling and a deramp FMCW radar further confirm the theory presented in this paper. A simple set of design equations is presented to allow reliable choice of the DDS frequency increment for a given level of the associated sidebands and for a given maximum range requirement.

In particular, a simple general design rule is proposed (the *−70 dBc rule*), $\Delta f = \sqrt{(B/1000T)}$, as a starting point to ensure that acceptable performance is obtained of −76 dBc (direct sampling) or −70 dBc (deramp) range sidebands due to the finite DDS frequency increment in an FMCW radar system. This design guideline will also be particularly useful for monolithic implementations of highly integrated FMCW radar designs incorporating custom DDS building blocks [16] where it would be advantageous to minimise the on-chip resource requirements.

AUTHOR CONTRIBUTIONS

Paul Victor Brennan: Conceptualization; formal analysis; investigation; methodology; writing – original draft. **Lai Bun Lok**: Experimental validation; writing – review & editing.

ACKNOWLEDGEMENTS

There has been no specific funding for this work.

CONFLICT OF INTEREST STATEMENT

We, the above authors, declare that we are not aware of any conflict of interest relating to the above paper and to its publication by the IET.

DATA AVAILABILITY STATEMENT

We, the above authors, are happy for the data and all content of this paper to be made available by the IET for Open Access or whatever means of dissemination is deemed appropriate.

ORCID

Paul Victor Brennan https://orcid.org/0000-0002-3145-3868

Lai Bun Lok https://orcid.org/0000-0002-0033-9173

REFERENCES

1. Jankiraman, M.: FMCW Radar Design. Artech House, Norwood p. 401. ISBN: 9781630815677. (2018)
2. Skolnik, M.: Introduction to Radar Systems, 3rd ed. McGraw-Hill p. 784. ISBN: 9780072881387. (2002)
3. Richards, M.A.: Fundamentals of Radar Signal Processing, 2nd ed. McGraw-Hill p. 618. ISBN: 9780071798327. (2014)
4. Bochkarev, D.N., et al.: Direct digital synthesizers of frequency and phase-modulated signals. In: IEEE 2019 Systems of Signal Synchronization, Generating and Processing in Telecommunications (SYNCHROINFO) (2019). https://doi.org/10.1109/SYNCHROINFO.2019.8814244
5. Murphy, E., Slattery, C.: 'All about direct digital synthesis', analog devices technical note. p. 5. https://www.analog.com/en/analog-dialogue/articles/all-about-direct-digital-synthesis.html (2004). Accessed 1 Jul 2022
6. Reinhardt, V.S.: Direct digital synthesisers. In: Proceedings of the 17th Annual Precise Time and Time Interval Systems and Applications, December 3–5, pp. 345–374 (1985)
7. Porqueras, F.M., Sole, A.A., Ibars, A.B.: Performance study of quantized linear frequency modulated signals and its application to CW radars. In: Proceedings 3rd European Radar Conference, pp. 100–103 (2006)
8. Peek, K.: An Analysis of the Effects of Digital Phase Errors on the Performance of FMCW-Doppler Radar. M.Sc. thesis. University of Twente p. 88 (2011)
9. Liu, P., et al.: Software-defined radar systems for polar ice-sheet research. In: IEEE Journal of Selected Topics in Applied Earth Observations and Remote Sensing, vol. 12(3), pp. 803–820 (2019). https://doi.org/10.1109/JSTARS.2019.2895616
10. Marks, R.J.: Handbook of Fourier Analysis and its Applications. Oxford University Press p. 744. ISBN: 9780195335927. (2009)
11. Brandwood, D.: Fourier Transforms in Radar and Signal Processing. Artech House p. 244(2011)
12. Taub, H., Schilling, D.L.: Principles of Communications Systems. McGraw-Hill p. 884. ISBN: 9780071003131. (1986)
13. 'AD9914 data sheet', analog devices. p. 45. www.analog.com/en/products/ad9914.html (2016). Accessed 1 Jul 2022
14. Brennan, P.V., et al.: Phase-sensitive FMCW radar system for high precision Antarctic ice shelf profile monitoring. IET Radar, Sonar Navig. 8(7), 776–786 (2014). https://doi.org/10.1049/iet-rsn.2013.0053
15. 'AD9910 data sheet', analog devices, p. 64. www.analog.com/en/products/ad9910.html (2016). Accessed 1 Jul 2022
16. Cali, J., et al.: A 650 MHz DDFS for stretch processing radar in 130nm BiCMOS process. In: 2013 European Microwave Integrated Circuit Conference, pp. 33–36 (2013)

How to cite this article: Brennan, P.V., Lok, L.B.: Choice and impact of frequency increment in direct digital synthesiser (DDS)-based linear FMCW radar. IET Radar Sonar Navig. 1–17 (2023). https://doi.org/10.1049/rsn2.12440